Electron-hole asymmetry in Co- and Mn-doped $SrFe_2As_2$

J. S. Kim,[1,*] Seunghyun Khim,[2] H. J. Kim,[1] M. J. Eom,[1] J. M. Law,[3,4] R. K. Kremer,[3] Ji Hoon Shim,[5] and Kee Hoon Kim[2,†]

[1]*Department of Physics, Pohang University of Science and Technology, Pohang 790-784, Korea*

[2]*CeNSCMR, Department of Physics and Astronomy, Seoul National University, Seoul 151-742, Korea*

[3]*Max-Planck-Institut für Festkörperforschung, Heisenbergstraße 1, D-70569 Stuttgart, Germany*

[4]*Department of Physics, Loughborough University, Loughborough LE11 3TU, United Kingdom*

[5]*Department of Chemistry, Pohang University of Science and Technology, Pohang 790-784, Korea*

(Received 23 March 2010; revised manuscript received 10 June 2010; published 15 July 2010)

Phase diagrams of electron- and hole-doped $SrFe_2As_2$ single crystals are investigated using Co and Mn substitution at the Fe sites. We find that the spin-density-wave state is suppressed by both dopants but the superconducting phase appears only for Co (electron) doping, not for Mn (hole) doping. Absence of the superconductivity by Mn doping is in sharp contrast to the hole-doped system with K substitution at the Sr sites. First-principles calculations based on detailed structural investigations reveal that a distinct structural change, i.e., the increase in the Fe-As distance by Mn doping is the most decisive factor to induce a magnetic and semiconducting ground state in $SrFe_{2-x}Mn_xAs_2$. The absence of electron-hole symmetry in the phase diagrams of the Fe-site doped $SrFe_2As_2$ suggests that the occurrence of high-T_c superconductivity is sensitive to the structural modification rather than the carrier doping.

DOI: 10.1103/PhysRevB.82.024510 PACS number(s): 74.70.Xa, 74.62.Dh, 74.25.Dw

I. INTRODUCTION

Whether or not an electron-hole symmetry holds for high-T_c cuprates has been an important issue for understanding the origin of high-T_c superconductivity.[1] Although the details of the doping dependence are different, both hole and electron dopings into the Mott-insulating parent compounds destroy the antiferromagnetic (AFM) ground state and eventually lead to high-T_c superconductivity. For the newly discovered high-T_c Fe pnictides,[2] such an electron-hole symmetry seems to be valid as demonstrated by several experiments so far.[3] In spite of the distinct *itinerant* AFM ground state[4] of the parent compounds, the phase diagram looks very similar with that of high-T_c cuprates; the superconducting phase boundary with a dome shape is formed at the region where the AFM phase is completely suppressed by both hole and electron doping. Understanding the common phase diagram of cuprates and Fe pnictides, therefore, is an essential step toward understanding their high-T_c superconductivity in the vicinity of the AFM phase.

Doping dependence of the electronic structure of Fe pnictides supports the electron-hole symmetry. Generally, the electronic structure of Fe pnictides near the Fermi level (E_F) consists of several bands mainly from Fe 3*d* orbitals hybridized with As *p* orbitals.[5,6] The undoped compounds show two different types of the Fermi surfaces (FS), hole pockets at the Γ point, and electron pockets at the *M* point in the Brillouin zone. They have almost the same size, leading to a spin-density-wave- (SDW-) type instability through strong interband nesting effects.[7,8] Upon hole doping, for example, the hole pockets grow while the electron pockets shrink, which in turn spoils the nesting condition for the SDW phase.[5] Once the SDW phase is suppressed sufficiently, the strong interband scattering is believed to provide important pairing channel for superconductivity.[7,9] For higher doping, however, the electron bands are completely emptied losing the interband pairing channel, and accordingly superconductivity is also suppressed with decrease of T_c.[10] Similar mechanism can be also operating in the electron doping regime,[11] which may lead to the electron-hole symmetry in the phase diagram.

The structure of the Fe pnictides consists of a common building block, the FeAs layer, and a charge reservoir layer, this being either a *RE*O layer (*RE*=rare earths) for the so-called "1111" compounds or an *AE* layer (*AE*=alkaline earths) for the "122" compounds. By modification of the charge reservoir or direct substitution at the Fe sites, additional charge carriers can be introduced into the FeAs layers. For example, in the 122 compounds, substitutions of Co,[11–16] Ni,[16–18] Pd, Rh, Ir,[19,20] and Pt[21] at the Fe sites cause electron doping while K substitution at the *AE* sites[22,23] or Mn substitution at the Fe sites[16] lead to hole doping. Among them, Mn doping shows a quite unique behavior; while all the other types of doings are successful for inducing superconductivity, Mn doping does not induce superconductivity. These findings suggest that not only the modulation of charge concentration but also other effects have to be taken into account for understanding the effects of doping.

Herein, we present the phase diagrams of electron- and hole-doped $SrFe_2As_2$ single crystals using direct substitutions of Co and Mn at the Fe sites. Similar to the case of K-doped $SrFe_2As_2$ at the Sr sites,[23] Mn doping at the Fe sites suppresses the SDW transition. However, Mn doping does not induce the superconductivity but rather makes the system more magnetic and insulating, revealing the absence of electron-hole symmetry in the phase diagram. We find that the structure is deeply related to the electron-hole asymmetry. Structural changes induced by K and Mn doping, in particular, the changes in the Fe-As distance turn out to be quite different. First-principles calculations also confirm that Mn-doped systems favor the magnetic ground state due to the larger Fe-As distance. Our results show that the superconductivity is not induced only by suppressing the SDW state but also by avoiding the strong increase in the Fe-As distance.

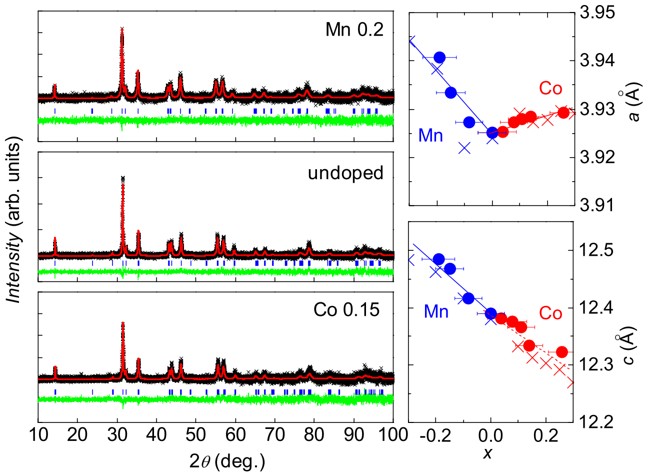

FIG. 1. (Color online) Typical x-ray powder-diffraction patterns using Cu $K\alpha$ radiation for (a) undoped, (b) Mn doped ($x=0.15$), and (c) Co doped ($x=0.15$) $SrFe_2As_2$. The red (dark gray) and black solid lines represent the Rietveld refinement and experimental data, respectively. The difference between the observed and the calculated data is shown by the solid line below the row of vertical bars marking the angles of the Bragg reflections used to simulate the patterns. Doping dependence of lattice constants (d) a and (e) c for $SrFe_{2-x}M_xAs_2$ (filled circle). For comparison, we also plot those of polycrystalline samples (Ref. 16) (cross).

II. EXPERIMENTAL AND THEORETICAL DETAILS

Single crystals of Co- and Mn-doped $SrFe_2As_2$ were grown using Sn-flux techniques as described in detail elsewhere.[15] X-ray diffraction (XRD) study on single crystals reveals sharp ($00l$) peaks, confirming a successful growth. In order to extract the structural information, we carried out XRD experiments using both Cu $K\alpha$ and Mo $K\alpha$ radiations in a Debye-Scherrer configuration, on powders made of individual single crystals. No additional diffraction peak has been detected, indicating good quality of the samples. The concentration of Co or Mn was determined by energy dispersive x-ray spectroscopy. The in-plane resistivity was measured by the standard four-probe method. Magnetization measurements were done under 7 T magnetic field along the ab plane using a superconducting quantum interference device magnetometer.

First-principles electronic-structure calculations are done by the full-potential linearized augmented plane-wave method implemented in WIEN2K code.[24] The local spin-density approximation is used for the exchange-correlation interaction. In order to describe the magnetic state, we construct supercell assuming each magnetic ground state with tetragonal structure obtained from experiments. Around 1000 k points are used for the full Brillouin-zone integration.

III. RESULTS AND DISCUSSIONS

Figure 1 shows the typical powder-diffraction patterns for undoped and Mn-/Co-doped $SrFe_2As_2$. Rietveld profile refinement was performed simultaneously for both XRD patterns taken with Cu $K\alpha$ and Mo $K\alpha$ radiations, based on the

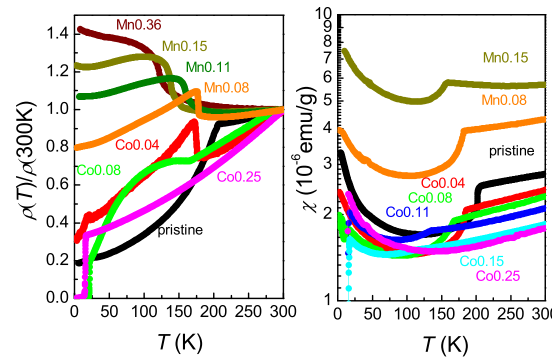

FIG. 2. (Color online) Temperature dependence of (a) the normalized resistivity $\rho(T)/\rho(300\ \mathrm{K})$ and (b) the magnetic susceptibility $\chi(T)$ at $H=7$ T along the ab plane for Co- and Mn-doped $SrFe_2As_2$.

space group of $I4/mmm$ using the program FULLPROF.[25] The converged parameters include the lattice constants, the fractional atomic position $(0,0,z)$ of the As $4e$ site, and isotropic thermal parameters for all atoms. The R_p, R_{wp}, and the reduced χ^2 are typically $\sim$3, 4, and 1.2, respectively. The c-axis lattice parameter shows a linear decrease from Mn to Co doping with ≈ 0.5 Å per doping (x), consistent with previous results on polycrystalline samples.[16] The in-plane lattice constant a slightly increases for both Co and Mn doping with a somewhat larger rate for Mn than for Co. Considering the ionic size of Mn^{2+}(0.66 Å), Fe^{2+}(0.63 Å), and Co^{2+}(0.58 Å),[26] we note that the nonmonotonous behavior of a with doping cannot be simply attributed to the different ionic size of the substituted atoms.

Figure 2 shows the normalized in-plane resistivity $\rho(T)$ and the in-plane magnetic susceptibility $\chi(T)$ in $SrFe_{2-x}M_xAs_2$ at $H=7$ T along the ab plane. A sudden drop in $\rho(T)$ and $\chi(T)$ in the parent $SrFe_2As_2$ at $T_{SDW}=205$ K corresponds to the SDW transition. Upon moderate Co doping, the anomaly in $\rho(T)$ becomes a sharp peak, which then shifts to lower temperatures and smears out with further Co doping. The kink in $\chi(T)$ also shifts to lower temperatures with doping, consistent with the behavior of $\rho(T)$. For $x \geq 0.04$, superconductivity is signaled by an abrupt decrease in $\rho(T)$ near 20 K and it is fully developed as a zero-resistivity state for $x \geq 0.08$. Below $x=0.15$, we found clear coexistence of the magnetic and superconducting transitions that has not been observed in polycrystalline samples.[14]

For Mn doping, on the other hand, the temperature dependences of $\rho(T)$ and $\chi(T)$ are quite different from those for Co doping. The anomaly of $\rho(T)$ and $\chi(T)$ due to the SDW transition shifts to lower temperatures as in Co doping but it becomes more pronounced with doping. Below T_{SDW}, $\rho(T)$ shows a much weaker temperature dependence, and upon further doping, $\rho(T)$ becomes almost temperature-independent at low temperatures indicating strong carrier localization. The overall magnitude of $\chi(T)$ increases with Mn doping while it becomes smaller with Co doping. Such behaviors in $\rho(T)$ and $\chi(T)$ for Mn doping are also in sharp contrast with the case of K doping. For K doping, the anomaly in $\rho(T)$ becomes weaker and $\rho(T)$ shows a more metallic behavior with doping before it eventually drops at

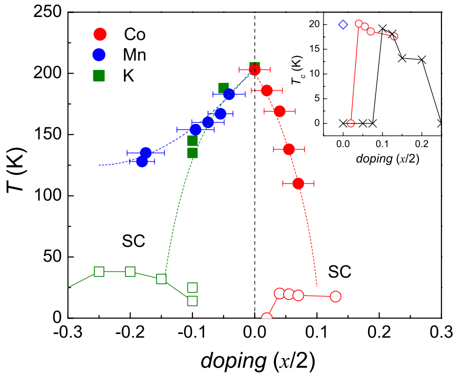

FIG. 3. (Color online) Phase diagrams of $SrFe_{2-x}M_xAs_2$ (M=Co and Mn) as a function of the number of extra conduction electrons per Fe with respect to the undoped system. The solid symbols indicate the AFM transition temperatures while the open ones represent the superconducting transition temperatures. Note that Mn doping does not induce the superconductivity while K doping does (Ref. 23). The inset shows the doping dependence of T_c for Co-doped $SrFe_2As_2$ single crystals (open circle). For comparison, together plotted are T_c of polycrystalline $SrFe_{2-x}Co_xAs_2$ in Ref. 14 (cross) and strain-induced $SrFe_2As_2$ in Ref. 27 (open diamond).

the superconducting transition.[23] These findings clearly demonstrate that Mn doping suppresses the SDW transition, similar to Co and K doping but drives the system to a distinct magnetic ground state different from the superconducting one.

The phase diagrams of $SrFe_{2-x}M_xAs_2$ determined from $\rho(T)$ and $\chi(T)$ are presented in Fig. 3. Here, we used the number of extra conduction electrons per Fe with respect to the undoped system, thus the negative value indicates hole doping. T_{SDW} was determined as the temperature where $\rho(T)$ begins to increase sharply or $\chi(T)$ shows a kink, which are in good agreement with each other. For comparison, T_{SDW} from K-doped $SrFe_2As_2$ is also shown.[23] T_{SDW} decreases monotonically with both types of doping and the decreasing rate is somewhat larger for electron doping than hole doping. The reduction in T_{SDW} can be understood in terms of the FS nesting effects. Since the SDW transition is closely related to the instability due to the strong FS nesting between hole and electron pockets, their size mismatch induced by electron or hole doping weakens the effects of the FS nesting. Similar doping dependence of T_{SDW} in low doping levels of K and Mn suggests that the size mismatch of the FS is crucial for determining T_{SDW}, irrespective to the type of dopant, until additional effects, e.g., structural modifications, play a significant role at higher doping levels.

Concerning the superconducting phase in the electron-doping side, both the magnetic and superconducting transitions were observed, suggesting the coexistence of two phases in the low doping regime. The doping dependence of T_c does not exhibit a clear dome shape as found in Co-doped $BaFe_2As_2$ (Ref. 11) but shows a steplike increase in T_c at low doping. In comparison with the polycrystalline data,[14] the Co-doping range for the superconducting phase is somewhat lower in single crystals. This discrepancy implies that the superconducting phase in doped $SrFe_2As_2$ is sensitive to the synthesis method, which may generate, e.g., different inter-

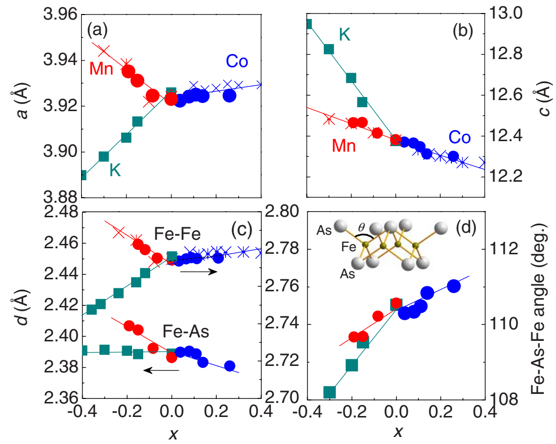

FIG. 4. (Color online) Doping dependence of lattice parameters (a) a and (b) c for Co, Mn, and K doping. The negative (positive) value of x indicates hole (electron) doping. The corresponding bond lengths of Fe with neighboring Fe and As and the bond angle around Fe with two neighboring As are shown (c) and (d), respectively. The local structure of the FeAs layer is shown in the inset of (d).

nal stress in the samples. In fact, recently Saha *et al.*[27] reported that even undoped $SrFe_2As_2$ can have a bulk superconductivity at 20 K. For the hole-doping side, K doping induces superconductivity above $x \approx 0.2$ while the superconducting phase is not observed for Mn doping up to $x \approx 0.4$. Note that this Mn doping level lies well inside the doping range where superconductivity is observed for K doping.

Having established the phase diagrams, we address why Mn doping does not induce the superconductivity while Co and K doping do. For the electron-doping regime, it has been found that various dopings with Co, Ni, Rh, and Pd result in exceptionally similar phase diagrams.[19] They match very well with each other when plotted as a function of electron density added by those dopants. The number of extra electrons has been proposed as the control parameter of the overall phase diagram, in particular, for the superconducting phase in the electron-doping regime.[19] This is, however, certainly not the case in the hole-doping regime as clearly seen by the distinctly different phase diagrams for K and Mn doping. In the hole-doping regime, the ground state is likely to be also determined by several other parameters such as subtle structural modification of the FeAs layer and the rearrangement of charge density due to different nuclear charge of the dopants. Clearly, an explanation of the phase diagrams in the hole-doped regime has to be sought beyond a rigid band picture.

Figure 4 shows several structural parameters by different types of dopings with K, Co, and Mn.[28] Comparing the doping dependence of the lattice parameters, we note that the in-plane lattice parameter a increases for Mn doping but it is rapidly reduced for K doping. For the c-axis lattice parameter, both Mn and K dopings results in the increase, but the increasing rate is much faster for K, which is partly understood as the ionic radius of K^+ (1.37 Å) is larger than that of Sr^{2+} (1.18 Å). Therefore, the corresponding Fe-Fe or Fe-As bond lengths are quite different, depending on the type of doping [see Fig. 4(c)]. For Co doping, the Fe-As distance decreases and the Fe-As-Fe angle becomes larger. Comparing Mn doping with K doping, the Fe-As-Fe angle is reduced in both cases, but with a somewhat larger rate for K doping. In addition, K doping reduces the Fe-Fe bond length but keeps the Fe-As length constant while Mn doping increases the both Fe-Fe and Fe-As bond lengths.

The bond distances and bond angles are closely related to the effective hoping amplitudes between the neighboring sites. The increase in the Fe-As bond length with the reduced Fe-As-Fe bond angle would make the hoping path of Fe-As-Fe less effective for Mn doping than K doping. Recent electronic-structure calculations[29–31] suggest that the Fe $3d$ bands with different orbital characters are entangled near the Fermi level and their relative position and the bandwidth are very sensitive to the hopping amplitudes between the nearest Fe neighbors. In particular, Fe $3d_{x^2-y^2}$ bands, whose contribution to the density of states (DOS) is quite large due to the almost dispersionless feature, are known to be easily shifted closer to the E_F by reducing the nearest-neighbor hopping. According to the Stoner criterion for itinerant magnets, formation of magnetic moment is governed by the parameter $N(E_F)I$, where I is a Stoner parameter. Therefore, the increase in the Fe-As distance by Mn doping is expected to favor the magnetic ground state because of the reduced Fe-As hopping and resultant larger contribution of narrow Fe $3d_{x^2-y^2}$ bands to the DOS. The calculated magnetic moment of $SrFe_2As_2$ is also expected to be enhanced as the Fe-As distance increases,[29] which is in good agreement with the experimental observations. As shown in Fig. 3(b), the overall magnitude of the susceptibility increases with Mn doping in $SrFe_2As_2$.

The Mn^{2+} itself, upon doping into $SrFe_2As_2$, is likely to favor a magnetic ground state. Mn^{2+} has a half-filled d shell with $3d^5$ configuration, thus it has stronger Hund's coupling than Fe^{2+} with $3d^6$ configuration. The spin-polarized states, therefore, would be expected in the MnAs system. In fact, recent investigations on $BaMn_2As_2$ revealed the checkerboard-type AFM state with a relatively high $T_N \approx 625$ K and the semiconducting behavior.[32] Electronic-structure calculations for $BaMn_2As_2$ also suggested strong spin-dependent hybridization between Mn d and As p states, leading to the AFM ground state.[33]

In order to elucidate a main deciding factor for the ground state among several candidates such as the change in carrier counts, the structural modification and the chemical nature of the dopant, we calculated the total energy of the SDW phase using first-principles calculations. In Fig. 5 we present the stabilization energy, namely, the difference of the total energies (ΔE) between those of the SDW phase (E_{SDW}) and the nonmagnetic phase (E_{NM}). Thus, when $-\Delta E$ becomes smaller, the magnetic phase is suppressed, whereas the increase in $-\Delta E$ means that the magnetism gets stronger. Other magnetic structures such as ferromagnetic or checkerboard-type AFM phases show similar tendencies but with smaller stabilization energies (not shown).

First, we consider the doping effects only [Fig. 5(a)]. In this case, we used the same crystal structure, i.e., the same lattice parameters and the same atomic position as $SrFe_2As_2$, except that E_F is shifted corresponding to the doping level of Mn and Co. The stabilization energy of the SDW phase, i.e.,

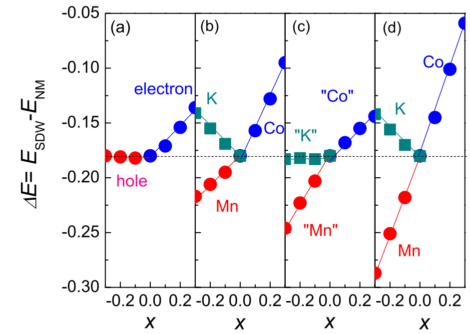

FIG. 5. (Color online) The calculated stabilization energies of the SDW states with respect to the nonmagnetic state for (a) $SrFe_2As_2$ with the shift of the chemical potential only, (b) K-, Mn- and Co-doped $SrFe_2As_2$, keeping the crystal structure same as pristine $SrFe_2As_2$, (c) undoped $SrFe_2As_2$ but assuming the crystal structure taken from K-, Mn- and Co-doped compounds, and (d) K-, Mn- and Co-doped $SrFe_2As_2$. Note that the negative (positive) value of x indicates hole- (electron) doping.

$-\Delta E$ is significantly reduced for electron doping indicating suppression of the magnetic state. By contrast, for hole doping, $-\Delta E$ remains almost constant. In terms of the FS nesting effects, both electron and hole dopings spoil the nesting conditions, thus relieving the electronic instability. However, doping dependence of the electronic DOS $[N(E_F)]$ is asymmetric between below and above the E_F; the $N(E_F)$ of $SrFe_2As_2$ strongly increases as the E_F is lowered while $N(E_F)$ is rapidly reduced when the E_F is moved to higher energies. This asymmetry originates from the fact that the electron pockets formed by the $3d_{xz/zy}$ bands with large bandwidth prevail above E_F. On the other hand, below E_F, the electronic structure is dominated by the narrow Fe $3d_{x^2-y^2}$ bands. Therefore, in addition to the degradation of the nesting conditions, the decrease in $N(E_F)$ in the electron-doped system favors the nonmagnetic states. For hole doping, however, the strong increase in $N(E_F)$ compensates the effects of degradation of the FS nesting conditions.

In the second step, we consider the effect of different nuclear charge of each dopant [see Fig. 5(b)]. Here we used the same crystal structure as the former case in Fig. 5(a) but taking into account of the effects of different dopant using a virtual crystal approximation. Thus, in this case, we consider the effects of the shift of the E_F plus the different nuclear charges of dopant. We also performed the supercell calculations for $x=0.25$, which gave consistent results (not shown). For electron doping, $-\Delta E$ is further reduced as compared to the case of the simple doping effect in Fig. 5(a). For the hole-doping side, different dopant gives different behavior; K doping reduces $-\Delta E$, suppressing the SDW phase, while Mn doping enhances $-\Delta E$, stabilizing the SDW phase.

In order to evaluate the effects of structural distortion only, we also calculated ΔE for a hypothetical $SrFe_2As_2$ with its crystal structure taken from those of K-, Mn-, and Co-doped samples. In this case, we keep the E_F same as the undoped compounds without any dopants. As shown in Fig. 5(c) $-\Delta E$ is significantly enhanced in the structure of Mn-doped samples while it stays almost constant in that of K-doped samples. This suggests that electronic structure,

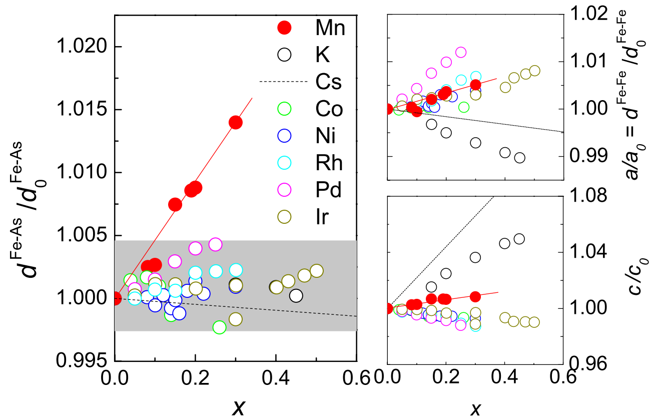

FIG. 6. (Color online) The doping dependence of (a) the Fe-As distance, (b) the Fe-Fe distance, and (c) c-axis lattice parameter for $Sr_{1-x}A_xFe_2As_2$ (A=K and Cs) and $SrFe_{2-x}M_xAs_2$ (M=Mn, Co, Ni, Rh, Pd, and Ir) as compared to those of pristine $SrFe_2As_2$. Note that except Mn (filled symbols), all other dopants (open symbols) induce superconductivity.

thus the ground state is sensitively affected by even a slight change in the structure (approximately a few percent). Combining all the effects of the chemical potential shift, the nature of dopant, and the structural distortion, ΔE as a function of doping is summarized in Fig. 5(d), which is roughly the sum of each contribution. For electron doping, most significant contribution for reducing the stabilization energy of the SDW phase comes from the shift of the E_F. The reduction in the Fe-As distance also makes a somewhat less but comparable contribution. For the hole-doping regime, the shift of the E_F does not affect much while the structural distortion, in particular, the increase in the Fe-As distance gives dominant contribution for stabilizing the SDW phase. We note that this behavior resembles the doping dependence of the Fe-As distance shown in Fig. 4(c). This implies that out of all structural parameters, the Fe-As distance is the most important control parameter for the formation of the magnetic phase, particularly in the hole-doping regime.

Bearing this in mind, we checked the change of the Fe-As distance[28] with various types of doping with K, Cs, Mn, Co, Ni, Rh, Pd, and Ir in literatures.[18,20,23,34–37] (see Fig. 6). These cover both electron and hole dopings, different doping sites (A sites and Fe sites), different valence (1+, 1−, and 2−), different period (3d, 4d, and 5d) as well as a wide range of ionic radius from 0.55 Å for Ni to 0.68 Å for Ir. The open symbols represent the dopants inducing superconductivity while the solid symbols correspond to the dopants that result in the nonsuperconducting phase. For lattice parameters a or c, their relative changes with respect to the pristine compound are quite random so that we cannot find any correlation with the (non) existence of superconductivity. In sharp contrast, for the Fe-As distance $d_{\text{Fe-As}}$, it is clear that only Mn doping not showing superconductivity leads to a strong increase in $d_{\text{Fe-As}}$ while all the other types of dopant inducing superconductivity results in almost negligible (less than 0.5%) variation in $d_{\text{Fe-As}}$. This observation, although it is empirical, is consistent with the results of first-principles calculations suggesting that the increase in the Fe-As distance is detrimental for inducing superconductivity and favors the magnetic ground states.

Recently, the effects of hole doping at the Fe sites have been investigated in $BaFe_{2-x}Cr_xAs_2$,[38,39] in which Cr^{2+} has a d^4 configuration, thus providing extra holes in the FeAs layers, similar to Mn^{2+} with d^5 configuration. Since Cr^{2+} has one less electron than the half-filled 3d shell of Mn^{2+}, one can expect that Cr^{2+} has a smaller magnetic moment, thus acting as a weaker magnetic impurity than Mn^{2+}. In terms of structural modification, on the other hand, Cr doping induces the increase in both lattice parameters a and c, reflecting strong covalency between Cr and As. This leads to the increase in the Fe/Cr-As bond distance similar to the Mn-doping case. The transport and magnetic properties as well as the resulting phase diagram for $BaFe_{2-x}Cr_xAs_2$ exhibit qualitatively the same doping dependence with those of $SrFe_{2-x}Mn_xAs_2$. These results, therefore, appear to be consistent with our conjecture that the structural distortion and the resulting magnetic interaction through the hybridization of transition metals and As is more important than the local magnetic configuration of the dopants.

In summary, using single crystals of a series of Co- and Mn-doped $SrFe_2As_2$, we explored the phase diagrams in the hole- and electron-doping regimes. Both types of doping suppress the SDW transition in the lower doping regime, but at higher doping levels, the resulting ground state is quite different: nonmagnetic and metallic state with superconductivity for Co but more magnetic and semiconducting state for Mn. The distinct physical properties of Mn-doped samples as compared to those of K-doped samples clearly demonstrate that for hole doping, the detailed nature of the dopant is important for inducing superconductivity. Based on the first-principles calculations, we show that slight doping-dependent structural change, in particular, the change in the Fe-As distance plays a key role for suppressing/stabilizing magnetic states. Such an exceptional sensitivity of the ground state to the small structural changes suggests that modifying electronic structures by structural distortions is more important than charge doping for inducing superconductivity.

ACKNOWLEDGMENTS

The authors thank Bing Lv for useful discussions and E. Brücher for experimental assistance. The work at SNU was supported by Korean government through Creative Research Initiatives, NRL (Grant No. M10600000238), GPP (Grant No. K20702020014-07E0200-01410), and Basic Science Research Programs (Grant No. 2009-0083512). The work at POSTECH was supported by the POSTECH Basic Science Research Institute Grant and by WCU through KOSEF (Grant No. R32-2008-000-10180-0). S.H.K. was supported by Seoul R & BD (Grant No. 10543).

*js.kim@postech.ac.kr
†optopia@snu.ac.kr

[1] As a recent review, see N. Armitage, P. Fournier, and R. Greene, arXiv:0906.2931 (unpublished).
[2] Y. Kamihara, T. Watanabe, M. Hirano, and H. Hosono, J. Am. Chem. Soc. **130**, 3296 (2008).
[3] K. Ishida, Y. Nakai, and H. Hosono, J. Phys. Soc. Jpn. **78**, 062001 (2009).
[4] J. Dong, H. J. Zhang, G. Xu, Z. Li, G. Li, W. Z. Hu, D. Wu, G. F. Chen, X. Dai, J. L. Luo, Z. Fang, and N. L. Wang, EPL **83**, 27006 (2008); C. de la Cruz, Q. Huang, J. W. Lynn, J. Li, W. Ratcliff II, J. L. Zarestky, H. A. Mook, G. F. Chen, J. L. Luo, N. L. Wang, and P. Dai, Nature (London) **453**, 899 (2008).
[5] Z. P. Yin, S. Lebe'gue, M. J. Han, B. P. Neal, S. Y. Savrasov, and W. E. Pickett, Phys. Rev. Lett. **101**, 047001 (2008).
[6] D. J. Singh and M. H. Du, Phys. Rev. Lett. **100**, 237003 (2008).
[7] I. I. Mazin, D. J. Singh, M. D. Johannes, and M. H. Du, Phys. Rev. Lett. **101**, 057003 (2008); I. I. Mazin and J. Schmalian, Physica C **469**, 614 (2009).
[8] M. M. Korshunov and I. Eremin, Phys. Rev. B **78**, 140509(R) (2008).
[9] K. Kuroki, S. Onari, R. Arita, H. Usui, Y. Tanaka, H. Kontani, and H. Aoki, Phys. Rev. Lett. **101**, 087004 (2008).
[10] T. Sato, K. Nakayama, Y. Sekiba, P. Richard, Y.-M. Xu, S. Souma, T. Takahashi, G. F. Chen, J. L. Luo, N. L. Wang, and H. Ding, Phys. Rev. Lett. **103**, 047002 (2009).
[11] L. Fang, H. Luo, P. Cheng, Z. Wang, Y. Jia, G. Mu, B. Shen, I. I. Mazin, L. Shan, C. Ren, and H.-H. Wen, Phys. Rev. B **80**, 140508(R) (2009).
[12] A. S. Sefat, R. Jin, M. A. McGuire, B. C. Sales, D. J. Singh, and D. Mandrus, Phys. Rev. Lett. **101**, 117004 (2008).
[13] J.-H. Chu, J. G. Analytis, C. Kucharczyk, and I. R. Fisher, Phys. Rev. B **79**, 014506 (2009).
[14] A. Leithe-Jasper, W. Schnelle, C. Geibel, and H. Rosner, Phys. Rev. Lett. **101**, 207004 (2008).
[15] J. S. Kim, S. Khim, L. Yan, N. Manivannan, Y. Liu, I. Kim, G. R. Stewart, and K. H. Kim, J. Phys.: Condens. Matter **21**, 102203 (2009).
[16] D. Kasinathan, A. Ormeci, K. Koch, U. Burkhardt, W. Schnelle, A. Leithe-Jasper, and H. Rosner, New J. Phys. **11**, 025023 (2009).
[17] L. J. Li, Q. B. Wang, Y. K. Luo, H. Chen, Q. Tao, Y. K. Li, X. Lin, M. He, Z. W. Zhu, G. H. Cao, and Z. A. Xu, New J. Phys. **11**, 025008 (2009).
[18] S. R. Saha, N. P. Butch, K. Kirshenbaum, and J. Paglione, Phys. Rev. B **79**, 224519 (2009).
[19] N. Ni, A. Thaler, A. Kracher, J. Q. Yan, S. L. Bud'ko, and P. C. Canfield, Phys. Rev. B **80**, 024511 (2009).
[20] F. Han, X. Zhu, P. Cheng, G. Mu, Y. Jia, L. Fang, Y. Wang, H. Luo, B. Zeng, B. Shen, L. Shan, C. Ren, and H. H. Wen, Phys. Rev. B **80**, 024506 (2009).
[21] S. R. Saha, T. Drye, K. Kirshenbaum, N. P. Butch, and J. Paglione, J. Phys.: Condens. Matter **22**, 072204 (2010).
[22] M. Rotter, M. Tegel, and D. Johrendt, Phys. Rev. Lett. **101**, 107006 (2008); M. Rotter, M. Pangerl, M. Tegel, and D. Johrendt, Angew. Chem., Int. Ed. **47**, 7949 (2008).
[23] K. Sasmal, B. Lv, B. Lorenz, A. M. Guloy, F. Chen, Y. Y. Xue, and C. W. Chu, Phys. Rev. Lett. **101**, 107007 (2008); M. Gooch, B. Lv, B. Lorenz, A. M. Guloy, and C. W. Chu, Phys. Rev. B **79**, 104504 (2009).
[24] P. Blaha, K. Schwarz, G. K. H. Madsen, K. Kvasnicka, and J. Luitz, in *WIEN2K*, edited by K. Schwarz (Technische Universitat Wien, Austria, 2001).
[25] J. Rodriguez-Carvajal, FULLPROF, version June 2005, ILL.
[26] R. D. Shannon, Acta Crystallogr., Sect. A: Cryst. Phys., Diffr., Theor. Gen. Crystallogr. **32**, 751 (1976).
[27] S. R. Saha, N. P. Butch, K. Kirshenbaum, J. Paglione, and P. Y. Zavalij, Phys. Rev. Lett. **103**, 037005 (2009).
[28] The Fe-As distance is determined by lattice parameters (a,c) and the atomic position of As (z). The a, c, and z values for our samples were determined from the Reitveld refinements (Fig. 1). For other compounds whose lattice parameters are available in the literature, but not the z value, we estimated z using the linear interpolation between two end points, those of $SrFe_2As_2$ and the compound with full substitution for a considering dopant. Such a linear dependence of z has been reported in various Fe pnictides, for example, $(Ba,K)Fe_2As_2$ (Ref. 22).
[29] M. J. Han, Q. Yin, W. E. Pickett, and S. Y. Savrasov, Phys. Rev. Lett. **102**, 107003 (2009).
[30] K. Kuroki, H. Usui, S. Onari, R. Arita, and H. Aoki, Phys. Rev. B **79**, 224511 (2009).
[31] V. Vildosola, L. Pourovskii, R. Arita, S. Biermann, and A. Georges, Phys. Rev. B **78**, 064518 (2008).
[32] Y. Singh, M. A. Green, Q. Huang, A. Kreyssig, R. J. McQueeney, D. C. Johnston, and A. I. Goldman, Phys. Rev. B **80**, 100403(R) (2009).
[33] J. An, A. S. Sefat, D. J. Singh, and M.-H. Du, Phys. Rev. B **79**, 075120 (2009).
[34] M. Noack and H.-U. Schuster, Z. Anorg. Allg. Chem. **620**, 1777 (1994).
[35] E. D. Bauer, F. Ronning, B. L. Scott, and J. D. Thompson, Phys. Rev. B **78**, 172504 (2008).
[36] A. Hellmann, A. Löhken, A. Wurth, and A. Mewis, Z. Naturforsch. **62b**, 155 (2007).
[37] W. K. Hofmann and W. Jeitschko, Monatsch. Chem. **116**, 569 (1985).
[38] A. S. Sefat, D. J. Singh, L. H. VanBebber, Y. Mozharivskyj, M. A. McGuire, R. Y. Jin, B. C. Sales, V. Keppens, and D. Mandrus, Phys. Rev. B **79**, 224524 (2009).
[39] S. L. Bud'ko, S. Nandi, N. Ni, A. Thaler, A. Kreyssig, A. Kracher, J.-Q. Yan, A. I. Goldman, and P. C. Canfield, Phys. Rev. B **80**, 014522 (2009).